The two-regime method for optimizing stochastic reaction–diffusion simulations

Mark B. Flegg*, S. Jonathan Chapman and Radek Erban

Mathematical Institute, University of Oxford, 24–29 St Giles', Oxford OX1 3LB, UK

Spatial organization and noise play an important role in molecular systems biology. In recent years, a number of software packages have been developed for stochastic spatio-temporal simulation, ranging from detailed molecular-based approaches to less detailed compartment-based simulations. Compartment-based approaches yield quick and accurate mesoscopic results, but lack the level of detail that is characteristic of the computationally intensive molecular-based models. Often microscopic detail is only required in a small region (e.g. close to the cell membrane). Currently, the best way to achieve microscopic detail is to use a resource-intensive simulation over the whole domain. We develop the two-regime method (TRM) in which a molecular-based algorithm is used where desired and a compartment-based approach is used elsewhere. We present easy-to-implement coupling conditions which ensure that the TRM results have the same accuracy as a detailed molecular-based model in the whole simulation domain. Therefore, the TRM combines strengths of previously developed stochastic reaction–diffusion software to efficiently explore the behaviour of biological models. Illustrative examples and the mathematical justification of the TRM are also presented.

Keywords: stochastic modelling; reaction–diffusion processes; multi-scale
simulation; hybrid algorithm

1. INTRODUCTION

Stochastic spatio-temporal simulations have been successfully used in a number of biological applications, including models of morphogen gradients [1], MAPK pathway [2], signal trasduction in *Escherichia coli* chemotaxis [3] and oscillation of Min proteins in cell division [4]. However, detailed stochastic spatio-temporal models are often computationally intensive to simulate. This is one of the reasons why whole cell simulation has been recognized as a 'grand challenge of the 21st century' [5]. In this paper, we address this problem using a modelling approach that has computational complexity only in regions of interest.

Spatio-temporal biological processes are often modelled using deterministic reaction–diffusion models that are written in the form of partial differential equations (PDEs) for concentrations of biochemical species [6]. However, cellular or subcellular processes usually take place on very small spatial scales. With such small scales, it is not uncommon for populations of biochemical species to be so small that deterministic (PDE-based) approaches are completely inappropriate. Several stochastic reaction–diffusion models have been introduced in the literature. In general, these models can be divided into two distinct classes [7]. The first class of models is compartment-based, which is characterized by a discretization of the spatial domain into compartments [8]. At any particular time, the best approximation to the localization of any individual molecule is the compartment that the molecule is in. Molecules that are in the same compartment and are of the same species are completely indistinguishable. Molecules are free to migrate in the form of discrete jumps from one compartment to another via diffusion. Compartment-based modelling techniques are very popular and are used in a number of available self-contained simulation packages, for example MesoRD [9] and SmartCell [10]. While compartment-based models do not specifically represent the true noisy trajectory of the molecules, it has been shown that these models can provide accurate results by choosing the mesh spacing carefully [11,12]. The second class of models is based on Brownian dynamics (molecular-based) simulation. The characterizing property of this method is that each molecule has an exact location on a continuous domain. Molecule diffusion is simulated by calculation of its noisy trajectory. There are a number of simulation packages that implement molecular-based simulation, for example Smoldyn [13,14], MCell [15,16] and Green's function reaction dynamics (GFRD) [17].

Brownian dynamics simulation is popular because of its better representation of the microscopic physics. However, if precise information about the trajectories of each molecule is not important, then the effort placed on tracking them is a waste of computational resources. As a general rule, if concentrations are really small, tracking every molecule's trajectory is achievable, but becomes less practical as concentrations increase, when compartment-based methods (or even deterministic methods)

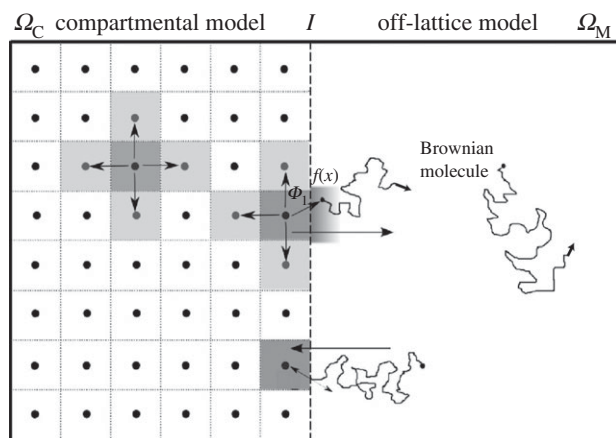*Author for correspondence (mark.flegg@maths.ox.ac.uk).

Figure 1. Graphical representation of the two-regime method.

are preferred. Often it is difficult to choose the most appropriate stochastic model when large spatial concentration variations, specific regions of interest and/or small systems coupled to larger systems are involved. In each of these cases, it would be ideal if a Brownian dynamics model may be used for localized regions of particular interest in which accuracy and microscopic detail is important (such as near the biological cell membrane [18]), and a compartment-based model may be used for other regions in which accuracy may be traded for simulation efficiency.

In this paper, we propose a spatially hybrid model, the two-regime method (TRM), which includes the best parts of each type of model and therefore optimizes simulation results. The TRM uses both a compartment-based approach and a molecular-based approach. It divides the computational domain Ω into two non-overlapping parts which we will label Ω_M and Ω_C, i.e. $\Omega = \Omega_M \cup \Omega_C$. Modellers compartmentalize that part of the domain in which they feel a compartment approach is best suited (labelled Ω_C in this paper) and consider molecules in Ω_M as free molecules diffusing and reacting on a continuous space using molecular-based modelling rules. Therefore, molecules jump from compartment to compartment in the spatially coarse regime in Ω_C and move according to Brownian motion in Ω_M with an exact location. The purpose of this paper is to outline the best way to couple these two regimes. That is, we address the following questions. Where and when does a molecule jump from a compartment in Ω_C into the molecular-based region Ω_M? And, how does a particle migrate from the molecular-based regime in Ω_M into a compartment in Ω_C? Both of these questions relate to the way in which molecules experience the interface between the two regimes that we will denote as I, i.e $I = \Omega_M \cap \Omega_C$. The schematic of the geometry of the TRM is shown in figure 1. To explain this method, we have to first summarize important facts about the compartment-based and molecular-based regimes. This will be done in §1.1 and §1.2. The TRM is then explained in full detail in §2.1.

1.1. Compartment-based modelling

The characterizing property of compartment-based stochastic models of reaction–diffusion processes is the

fact that the domain is discretized. Molecules do not have exact locations as they do in Brownian dynamics simulations, but rather they are only assigned to be located within one of the compartments at a given moment in time. In particular, computer implementations of compartment-based models only store and evolve numbers of molecules in compartments (for each biochemical species). In what follows, we will consider the discretization of the computational domain using the compartments of the same size. This means that, in the case of three-dimensional simulations, compartments will be small cubes with the side equal to h. Similarly, compartments will be squares with the side h (respective intervals of length h) for two-dimensional (respectively one-dimensional) models. In each case, diffusion is modelled by allowing jumps of molecules between neighbouring compartments with rate D/h^2, where D is the diffusion constant [19].

Compartment-based models postulate that chemical reactions only occur if the reactant molecules are in the same compartment [9]. Let us consider a general system of N chemical species that are subject to M chemical reactions in a domain Ω_C that is discretized into K compartments. Then compartment-based models assign a propensity function $\alpha_{i,j}(t)$, $i = 1, 2, \ldots, M$, $j = 1, 2, \ldots, K$, to each chemical reaction in each compartment. Here, the product $\alpha_{i,j}(t)dt$ is the probability that the i-th chemical reaction occurs in the j-th compartment during the infinitesimally small time interval $[t, t + dt]$. The propensity $\alpha_{i,j}(t)$ depends on the number of available reactants in the compartment, the kinetic rate constant and the compartment size h [7]. In a similar way, one can assign the propensity of diffusive jumps from the j-th compartment, $j = 1, 2, \ldots, K$, to its neighbouring compartments to be $\alpha_{i,j}(t) = D/h^2$, where $i = M+1, \ldots, M + d_j$ and d_j is the number of available compartments adjacent to the j-th compartment. In this way, the reaction events and the diffusive jumps are both contained in the propensities $\alpha_{i,j}$.

Because a real diffusing molecule's trajectory is continuous, if a molecule leaves a compartment, it enters a neighbouring compartment. This necessarily places a constraint on the time step in which the system is updated. Commonly, there are two separate ways of simulating molecule migration from compartment to compartment. The first is by designation of the time step Δt [20]. We will call this the *time-driven* approach. This is a less accurate, but simpler, method of simulation. Regardless of how small the time step is, there will be a non-zero probability for molecules to move more than one compartment, which leads to inaccuracies in the results. However, accuracy is assured so long as the probability for a single molecule to move just one compartment, $D\Delta t/h^2$, is small (which makes the probability for two compartment jumps negligible). Further restrictions on the time step might also be provided by fast chemical reactions.

A more common approach to compartment-based modelling is given by *event-driven* algorithms, which simulate the evolution of the system by picking the time step that corresponds to the next diffusive jump or reaction event [21,22]. Examples include the Gillespie algorithm [21], next reaction method [22] and

next subvolume method [9]. In the next reaction method, the time $t + \tau_{i,j}$ for each reaction and diffusion jump is computed putatively by

$$\tau_{i,j} = \frac{1}{\alpha_{i,j}} \ln\left(\frac{1}{r_{i,j}}\right), \qquad (1.1)$$

where $r_{i,j}$ is a uniformly distributed random number in $(0,1)$. In particular, if the compartment size h is reduced, then the propensities D/h^2 of the molecules to migrate between compartments increases, which causes the time step between diffusive events to decrease in turn. Thus, in both time-driven and event-driven algorithms, the time step and the compartment size are inherently linked (either by the constraint of small jumping probabilities or by correlation between the randomly selected time step and the compartment size).

1.2. Molecular-based modelling

Computer implementations of molecular-based models in the literature store and evolve the positions of all biomolecules of interest [13]. The trajectories of large biomolecules (proteins) are computed through Brownian dynamics [23]. This is done by the inclusion of a random motion term that models the effect of solvent molecules on the biomolecules of interest without the need to simulate each solvent molecule individually. In the time-driven algorithms, the position $\mathbf{x}_i(t + \Delta t)$ of the i-th molecule at time $t + \Delta t$ is computed from its position $\mathbf{x}_i(t)$ at time t by

$$\mathbf{x}_i(t + \Delta t) = \mathbf{x}_i(t) + \sqrt{2D\Delta t}\,\boldsymbol{\zeta}, \qquad (1.2)$$

where $\boldsymbol{\zeta} = [\zeta_x, \zeta_y, \zeta_z]$ is a vector of three normally distributed random numbers with zero mean and unit variance. Chemical reactions are then performed at each time step according to the probability of each reaction. Probabilities of bimolecular reactions also depend on the distance of possible reactants [7,13]. Molecules that migrate over domain boundaries are treated depending on whether they are reflective, absorbing or reactive boundaries [18].

A time-driven Brownian model is simple to implement, but may not be efficient. Prescribing a time step Δt to an arbitrary simulation can be difficult because if the concentration is too small, then many time steps will be calculated before any interactions or interesting features may take place. Sometimes event-driven algorithms are preferred for Brownian dynamical models. An example is the GFRD method [17] that chooses a time step based on the current system configuration. It makes use of the fact that single-particle and two-particle problems can be solved analytically using Green's functions, and selects the time step in such a way that the system evolution can be approximated as a collection of two-particle (or single-particle) problems.

2. RESULTS

2.1. Two-regime method

The TRM is a spatially hybrid model for stochastic reaction–diffusion processes that uses a two-part domain Ω. One part, Ω_{C}, is discretized into compartments and

the other, Ω_M, is a molecular-based subdomain ($\Omega = \Omega_{\mathrm{C}} \cup \Omega_{\mathrm{M}}$). The interface between the subdomains is denoted as $I \equiv \partial\Omega_{\mathrm{C}} \cup \partial\Omega_{\mathrm{M}}$. The algorithm is graphically presented in figure 1. Some details of the implementation of TRM are dependent on the choice of algorithms governing each individual regime, i.e. whether we use a time-driven or event-driven approach in Ω_{C} and Ω_{M}. In this section, we focus on the most common case. Other cases are discussed in §3.

Commonly, compartment-based stochastic reaction–diffusion models are implemented using an event-driven algorithm [9], while molecular-based stochastic reaction–diffusion models are implemented using a time-driven approach [13]. We therefore present the TRM that integrates an event-driven compartment-based reaction–diffusion regime (next reaction method [22]) and a time-driven molecular-based reaction–diffusion regime (for example, that used by Smoldyn [13]). The algorithm is summarized in table 1.

Molecules in both Ω_{C} and Ω_{M} are simulated according to the rules defined by their particular algorithm. Therefore, when initializing in step (i), molecules are placed according to compartment in Ω_{C} and according to coordinate in Ω_{M}. The propensity for molecules to migrate from compartments adjacent to the interface I into Ω_{M} is given by $\Phi_1 D/h^2$ per molecule, where Φ_1 is the change in the propensity of migration (from that of an internal migratory event) that is included to make the molecular flux over the interface I consistent with diffusion. We have determined Φ_1 to be (see appendix A)

$$\Phi_1 = \frac{2h}{\sqrt{\pi D \Delta t}}, \qquad (2.1)$$

where Δt is the fixed time increment defined for updating the molecules in Ω_{M}. We use (1.1) to find the putative times $t + \tau_{i,j}$ for the next reaction/migration events in Ω_{C}. We call these *C-events*. They include the jumps from Ω_{C} to Ω_{M}, which have propensities equal to $\Phi_1 D/h^2$ multiplied by the number of molecules in the corresponding compartment. Therefore, we define d_j to be the number of available directions in which a molecule may jump, including a jump over the interface I. In step (ii), we also initialize the time of the next update of molecules in Ω_{M} as $t_{\mathrm{M}} = \Delta t$ (we call these *M-events*).

The algorithm then proceeds by repeating steps (iii) and (iv), which compute *C-events* and *M-events* respectively. At each *C-event*, we track the reaction-migratory events that occur in Ω_{C}. At each *M-event*, we update the entire system of molecules in Ω_{M} by calculating the new positions of molecules in Ω_{M} using (1.2) and the reactions using the method prescribed by the specific molecular-based algorithm [13,23]. At each *M-event*, we also introduce new molecules from Ω_{C} into Ω_{M} by placing them at a distance x from the interface I that is sampled from the probability distribution $f(x)$. These new molecules arise from those *C-events* that have occurred since the previous *M-event*. We have determined that (see appendix A)

$$f(x) = \sqrt{\frac{\pi}{4D\Delta t}}\,\mathrm{erfc}\left(\frac{x}{\sqrt{4D\Delta t}}\right), \qquad (2.2)$$

Table 1. The two-regime method (TRM) for stochastic reaction–diffusion simulation.

(i) Initialize numbers of molecules in compartments in Ω_C and positions of molecules that are in Ω_M.

(ii) Choose Δt, the time between updates of the molecular-based regime (M-events) in Ω_M. Use (1.1) to calculate $\tau_{i,j}$, the putative times at which the next reaction or migratory events (C-events) will take place in Ω_C (or are initiated in Ω_c for jumps over the interface I). Set $t_M = \Delta t$ and $t_C = \min(\tau_{i,j})$, where the minimum is taken over all $i = 1,2,\dots,M + d_j$ and $j = 1,2,\dots,K$.

(iii) If $t_C \leq t_M$, then the next C-event occurs:
— Update current time $t := t_C$.
— Change the number of molecules in Ω_C to reflect the specific C-event that has occurred. If this event is one in which a particle leaves Ω_C bound for Ω_M, then compute its initial position in Ω_M according to the method described in the text (using (2.2)) and remove it from the corresponding compartment adjacent to the interface I. Calculate the next putative time for the current C-event by (1.1).
— For all propensity functions $\alpha_{i,j}$ that are changed as a result of the C-event, determine the putative times of the corresponding event by (2.4).
— Set $t_C := \min(\tau_{i,j})$.

(iv) If $t_M \leq t_C$, then the next M-event occurs:
— Update current time $t := t_M$.
— Change the locations of all molecules in Ω_M according to (1.2).
— Initialize all molecules which migrated from Ω_C to Ω_M during previous C-events at locations computed in step (iii), using (2.2).
— Perform all reaction events in Ω_M.
— Absorb all molecules that interact with the interface I from Ω_M (excluding those just initiated) into the corresponding compartment in Ω_C (or into the compartment which is closest to their final calculated position). The molecules moving across the interface are selected with the help of (2.3).
— For all propensity functions $\alpha_{i,j}$ that are changed as a result of the M-event determine the putative times of the corresponding C-event by (2.4).
— Update $t_M := t_M + \Delta t$ and, if necessary, set $t_C := \min(\tau_{i,j})$.

(v) Repeat steps (iii) and (iv) until the desired end of the simulation.

---

where $x \geq 0$ is the distance from the boundary, and $\mathrm{erfc}(x) = 2/\sqrt{\pi} \int_x^\infty \exp(-\xi^2)\,d\xi$ is the complementary error function. To sample efficiently from this distribution, one can follow the method presented in Andrews [24, eqn (35)]. Note that the probability distribution (2.2) can also be interpreted as a concentration profile created by diffusion over the period of Δt from initial concentration given as a Heaviside function [25]. This implies that the molecular-based algorithm 'senses' the compartment as a continuous, uniform, distribution of particles rather than a single source of particles originating at the node of the compartment or any other specific microscopic arrangement.

In step (iv), we also identify all molecules that migrate from Ω_M to Ω_C during an M-event. These include those molecules which have new locations calculated by (1.2) in Ω_C. However, we also have to include some molecules that have their new locations calculated by (1.2) in Ω_M. In appendix A, we show that every molecule has a probability P_m to migrate from Ω_M to Ω_C during an M-event where

$$P_m = \exp\left(\frac{-\Delta x_{\mathrm{old}}\,\Delta x_{\mathrm{new}}}{D\Delta t}\right), \qquad (2.3)$$

where Δx_{old} is the distance of the molecule from the interface I before the M-event and Δx_{new} is the calculated distance from the interface I at the current M-event. All molecules that migrate from Ω_M to Ω_C

are placed into the corresponding (nearest) compartment in Ω_C. It is worth noting that (2.3) is also used in some stochastic reaction–diffusion algorithms for the treatment of boundary conditions [13,18]. In the TRM, the external (physical) boundary conditions are implemented for each regime in the usual way (e.g. [18]), where treatment of reflective, absorbing and reactive boundaries is discussed. Furthermore, it is also worth noting that implementation of absorbing molecules implicitly (using (2.3)) is very costly numerically. If one were to simply allow transfer of molecules based on whether or not they appear on the other side of the interface, an error proportional to the net flux over the interface would be the result.

For both C-events and M-events, when the propensity $\alpha_{i,j}$ is changed owing to a change in Ω_C, we must recalculate the putative time $t + \tau_{i,j}$ for the next C-event to take place. Following Gibson & Bruck [22], we update $\tau_{i,j}$ as follows:

$$\tau_{i,j} := t + \frac{\alpha_{i,j}^{\mathrm{old}}(t)}{\alpha_{i,j}^{\mathrm{new}}(t)}(\tau_{i,j} - t), \qquad (2.4)$$

where $\alpha_{i,j}^{\mathrm{old}}(t)$ is the propensity before the event at time t and $\alpha_{i,j}^{\mathrm{new}}(t)$ is the propensity after the event.

Migratory events from compartments into Ω_M occur at C-events. Until they are initialized, they have no probability of interaction or reaction. The probability of reaction is calculated after the initialization at the

next *M*-event depending on its initialized position in comparison with other molecules that it may interact with. This consideration does not affect the accuracy of the algorithm because the time between a *C*-event and the subsequent *M*-event is small (smaller than Δt).

Mathematical justification of the TRM is given in appendix A. In order to demonstrate the validity of the TRM, we will present results for two test problems for which one can derive analytically the exact solution. We can therefore test our stochastic simulation by increasing the number of realizations and observing convergence between the exact solution and the stochastic simulation. The first test problem is presented in §2.2. It has been designed so that a large range of different concentrations and fluxes will exist at some stage on and across the interface so that theoretical agreement will provide more compelling validation of the algorithm in all possible situations. In §2.3, we will apply the TRM to a particular model of protein concentration gradients in order to demonstrate the usefulness of the TRM to an existing biological model [26].

2.2. Illustrative results: diffusion example

We will consider one-dimensional diffusion of N_0 non-interacting molecules with diffusion constant $D = 1$ in the domain $\Omega = [0,1]$. In this example, all parameters are dimensionless. The boundaries of the domain Ω are defined to be reflective. We assume that initially all molecules are uniformly distributed in the subinterval $[0,0.5]$. Physically, this problem is nothing other than the diffusion of molecules squashed into half a room being suddenly allowed to fill the room. This problem can be stated as the following initial boundary value problem for the (normalized) density ϱ of molecules

$$\frac{\partial \varrho}{\partial t} = \frac{\partial^2 \varrho}{\partial x^2}, \quad 0 < x < 1, \tag{2.5}$$

where $\varrho(x,0) = 2H(0.5 - x)$, $\varrho_x(0,t) = \varrho_x(1,t) = 0$ and H is the Heaviside function. The solution can be found by applying the separation of variables technique to (2.5) as

$$\varrho(x, t) = 1 - 4 \sum_{i=1}^{\infty} \frac{(-1)^i \cos((2i-1)\pi x)}{(2i-1)\pi}$$
$$\times \exp(-(2i-1)^2 \pi^2 t). \tag{2.6}$$

This solution will be used to test the validity of the TRM.

To apply the TRM, we divide Ω into the following compartment-based and molecular-based parts: $\Omega_C = [0,0.5]$ and $\Omega_M = [0.5,1]$. Therefore, the interface I is located at $I = \partial \Omega_C \cap \partial \Omega_M = \{0.5\}$. The compartment-based domain Ω_C is discretized into $K = 20$ compartments (subintervals) of the length $h = 0.025$. The compartment-based model will give us the time evolution of a vector of integers $\mathbf{n} = [n_1, n_2, \ldots, n_K]$, where n_i is the number of molecules in the i-th compartment, $i = 1, 2, \ldots, K$. Initially, all N_0 molecules are
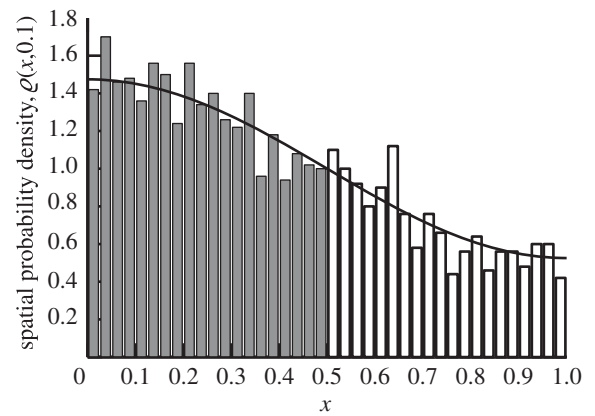

Figure 2. The TRM applied to the diffusion example which was introduced in §2.2. We plot the spatial distribution of molecules at time $t = 0.1$ according to (2.6) (black line) and TRM (compartment molecule probability density shown in dark compartment bars and free molecules counted into compartments and shown in white bars). The compartmental separation is $h = 0.025$.

placed in Ω_C in random compartments with equal probability. This constitutes step (i) in table 1. In step (ii), we choose the time step Δt as $\Delta t = 10^{-6}$; therefore, Φ_1 given by (2.1) is approximately 28.

Figure 2 is a plot of the distribution comparing the solution (2.6) and the distribution that is produced using our stochastic algorithm at $t = 0.1$. We use $N_0 = 2000$ molecules in these simulations. For comparative purposes, the molecules in Ω_M are counted and compartmentalized so that we can see their relative concentration to that of the compartments in Ω_C. While good agreement is observed, we require a more quantitative comparison. It has been established in the literature that the algorithms that govern the internal processes of Ω_M and Ω_C are consistent with diffusion, and therefore we are most interested with the accuracy of the flux over the boundary. For this reason, we compare the total probability to find molecules in Ω_C with that predicted by (2.6) (i.e. $\int_0^{0.5} \varrho(x,t) dx$). A comparison of a theoretical probability and simulation containing $N_0 = 2000$ molecules shows good agreement over time in figure 3. Simulation of the TRM with $N_0 = 3 \times 10^4$ overlaps that of the theory in figure 3. Thus, in figure 4, we present a plot of the error between the expected probability to find molecules in Ω_C and that of a simulation with $N_0 = 3 \times 10^4$ molecules over time to demonstrate that there is no apparent time-dependent error that is associated with the algorithm; rather, there are unbiased fluctuations around the true expected probability. The test problem, therefore, provides very strong validation of the proposed algorithm.

2.3. Morphogen gradient model

In the second test problem, we simulate a model of a diffusing morphogen presented by Tostevin *et al.* [26]. Consider a system of no molecules on the semi-infinite domain $\Omega = [0,\infty)$. Morphogen molecules are produced at the origin $x = 0$ at a rate $J = 6.25$ μm^{-1} s^{-1} and diffuse with a diffusion coefficient of $D = 0.5$ μm^2 s^{-1}. We implement a zero flux boundary condition at the origin.
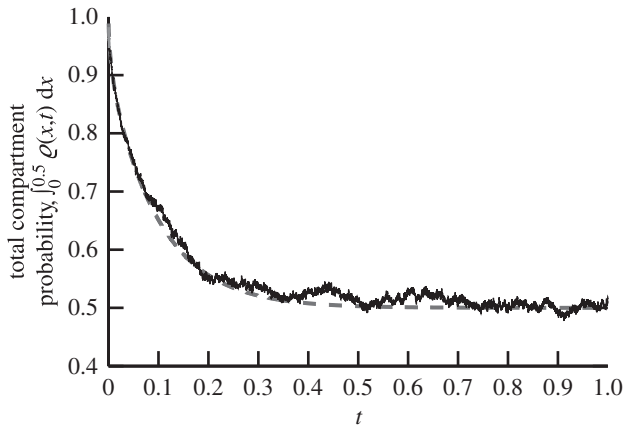
Figure 3. Plot of total probability to find a particle bound to a compartment as a function of time ($\int_0^{0.5}\varrho(x,t)\mathrm{d}x$) according to (2.6) (grey dashed line) and from simulation of 2000 molecules (solid black line) using the TRM for the diffusion example from §2.2.
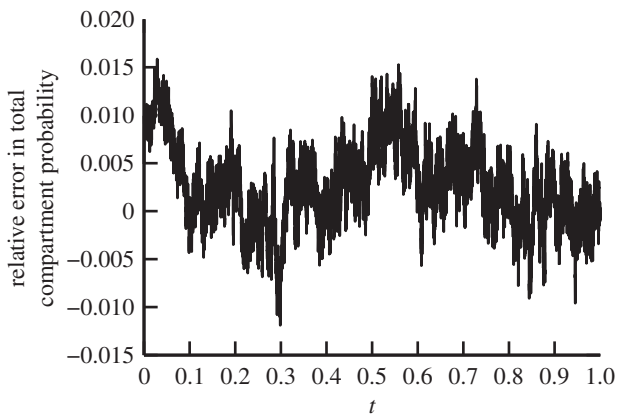

Figure 4. Relative stochastic error of the total probability to find a particle bound to a compartment ($\int_0^{0.5}\varrho(x,t)\mathrm{d}x$) between simulation of the diffusion example (given in §2.2) using the TRM with 3×10^4 molecules and the theoretical value calculated using (2.6), as a function of time.

The molecules undergo decay with rate $\mu = 1$ s^{-1}. Intuitively, because molecules are produced only at the origin and decay as they diffuse away from the origin, there will be a large concentration of molecules near the origin that dissipate as x gets large. If a molecular-based algorithm were to be used for this model, at small values of x, where there are characteristically a lot of molecules, high computational effort will be needed, whereas accurate and efficient results are achievable using a compartment-based model. However, using a compartment-based algorithm for the entire model would mean necessarily truncating the domain and introducing errors associated with small concentrations at large values of x. This type of problem is ideal for the TRM because we would prefer to use the efficiency of a compartment-based model for small x and the precision of a molecular-based model for large x. We, therefore, simulate the model using the TRM and place the interface at an arbitrarily chosen location ($x = 1$ μm). Therefore, $\Omega_\mathrm{C} = [0,1)$ and $\Omega_\mathrm{M} = [1,\infty)$. In
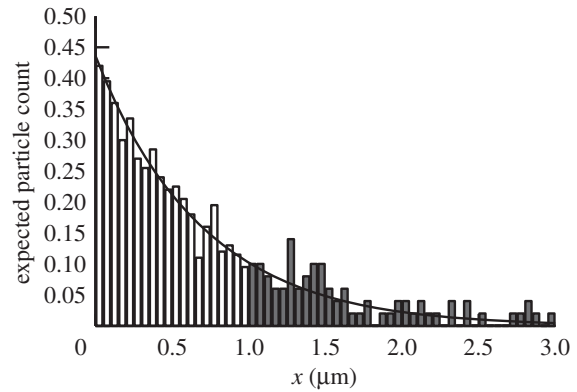

Figure 5. The TRM applied to the morphogen gradient model that was introduced in §2.3. Plot of the expected morphogen molecule count per compartment evaluated at $t = 3$ s according to (2.8) (black line) and 200 realizations of the TRM simulation (compartment molecule probability density shown in white compartment bars and free molecules counted into compartments and shown in dark bars).

the large J limit, we expect the concentration of molecules, $\varrho(x,t)$ to obey the PDE

$$\frac{\partial \varrho}{\partial t} = D\nabla^2\varrho - \mu\varrho + J\delta(x), \quad x > 0, \qquad (2.7)$$

where $\delta(x)$ is the Dirac delta function. While there is zero flux over the boundary, the introduction of the point source term at $x = 0$ gives us a formal boundary condition of $\varrho_x(0,t) = -J/D$. The initial condition is $\varrho(x,0) = 0$. The time-dependent analytical solution is given by Bergmann *et al.* [27]

$$\varrho(x,t) = \frac{\lambda J \exp(-x/\lambda)}{2D}\left[1 - \frac{1}{2}\mathrm{erfc}\left(\frac{2Dt/\lambda - x}{\sqrt{4Dt}}\right)\right.$$
$$\left. + \frac{-\exp(2x/\lambda)}{2}\mathrm{erfc}\left(\frac{2Dt/\lambda + x}{\sqrt{4Dt}}\right)\right],$$
$$(2.8)$$

where $\lambda = \sqrt{D/\mu}$ is the characteristic decay length. Using this analytical solution, we can discuss the accuracy of the TRM by combining 5000 simulations of this problem.

We chose the following parameters for our simulation results; $\Delta t = 0.1$ ms for the molecular-based model and $h = 0.05$ μm for the compartment-based model. Figure 5 is a plot of the distribution comparing the analytical solution (2.8) and the distribution that is produced using our stochastic algorithm averaged over 5000 realizations at time $t = 3$ s. In order to test that the interface properties of the TRM are accurate, we compare $\int_0^1 \varrho(x,t)\mathrm{d}x$ computed by (2.8) with the total number of compartment-bound molecules averaged over 5000 simulations and $\int_1^\infty \varrho(x,t)\mathrm{d}x$ with the total number of molecules in Ω_M averaged over the same 5000 simulations. The results are shown in figure 6. The stochastic and analytical results are in clear agreement.

3. DISCUSSION

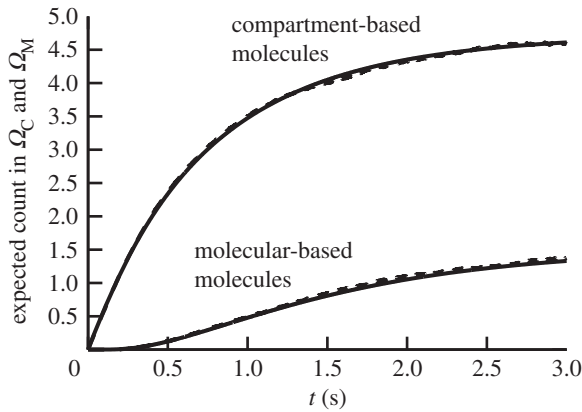In this manuscript, we have successfully interfaced a compartment-based model of diffusion to a Brownian

Figure 6. Plot of total expected number of morphogen molecules found in both Ω_C and Ω_M as a function of time for the analytical solution according to (2.8) (solid lines) and TRM simulation results averaged over 5000 realizations (dashed lines).

dynamics model of diffusion. We have derived and verified, for any process that has diffusion as its dominant form of molecule mobility, very particular rules in which molecules may freely migrate between a compartment-based regime and a free Brownian dynamics regime. The ability to interchange the modelling approach in spatially specific areas allows greater control in simulation and in particular allows a modeller to have the precision of a molecular-based regime in regions where it is needed, while having the computational efficiency of compartment-based approaches where it is appropriate. In order to interface the two regimes, one simply needs to migrate molecules between regimes according to the rules described in table 1 and using the coupling parameters given in equations (2.1) and (2.2). Their mathematical justification is given in appendix A.

It is important to note that, while we have focused on presenting the TRM using an event-driven compartment-based regime and a time-driven molecular-based regime, it is possible to use any desired combination of compartment-based and molecular-based regimes. In the case where algorithms in both Ω_C and Ω_M are event-driven (for example, using the GFRD [17] in Ω_M), the parameters Φ_1 and $f(x)$ are the same. Care must be taken in this case. Molecule migration from Ω_M to Ω_C occurs at the moment of first contact with the interface *I*. Furthermore, equation (2.1) implies that (in the case of an event-driven algorithm) Φ_1 is dependent on $\tau_{i,j}$, which in turn determines the propensity for the diffusive events on interfacial compartments in Ω_C and therefore determine $\tau_{i,j}$ itself. The putative time for the migration of a particle from the boundary compartment in Ω_C to Ω_M is calculated from some current time in the following way:

$$\tau_{i,j} = \frac{h^2}{n_b \Phi_1 D} \ln\left(\frac{1}{r}\right), \qquad (3.1)$$

where n_b is the number of molecules in the compartment at the interface and r is a uniformly distributed random number in (0,1). Notice from (2.1) that $\Phi_1\sqrt{\tau_{i,j}}$ is equal to $2h/\sqrt{\pi D}$, which is a constant with

respect to $\tau_{i,j}$. Therefore, using (3.1), we find that $\tau_{i,j}$ can be computed by the following formula:

$$\tau_{i,j} = \left(\frac{h^2}{n_b(\Phi_1\sqrt{\tau_{i,j}})D}\ln\left(\frac{1}{r}\right)\right)^2 = \frac{\pi h^2}{4n_b^2 D}\ln^2 r. \quad (3.2)$$

The illustrative algorithms that we presented were effectively one-dimensional, but the algorithm naturally extends by symmetry into higher dimensions with flat interfaces. It still remains to extend the work into curved higher dimensional interfaces and systems with advection as a form of molecule mobility. Another important extension is to consider unstructured meshes [28] and complex geometries [29]. We are currently working on these important extensions and we will report our findings in a future publication. The presented algorithm has the potential to significantly increase the accuracy and speed at which stochastic reaction–diffusion simulations are implemented by giving the simulator control over modelling approaches in specific regions of interest.

APPENDIX A. DERIVATION OF PARAMETERS (2.1)–(2.3)

In this appendix, we derive equations (2.1) and (2.2), i.e. we derive equations relating the TRM parameters Φ_1 and $f(x)$ and the parameters of compartment-based and molecular-based models. This derivation will also make use of an auxiliary parameter Φ_2 (which does not explicitly appear in the formulation of the TRM, because its value is determined to be equal to 2 in all cases). We also justify equation (2.3).

Without loss of generality, consider an interface at $x = 0$. To the left of this interface, a compartment-based model is used with fixed compartment size h. To the right of the interface, a molecular-based algorithm is used, updated at fixed time increments of Δt. Our aim is to choose the parameters that govern the transfer of molecules across the interface from one model to the other in such a way as to make the interface 'invisible' in the solution: the switch of models does not reflect anything in the underlying physical processes, it is simply a mathematical construct to aid the simulation.

To determine these parameters, we focus on the purely diffusive problem, because bulk reactions have no effect on boundary conditions [18]. Then the exact description of the underlying physical problem is a set of *N* molecules undergoing Brownian motion. We write $\bar{p}(x,t)$ for the distribution function for this process, so that $\bar{p}(x,t)\,\mathrm{d}x$ gives the probability of finding a given molecule in the interval $[x, x + \mathrm{d}x]$ at time t. In the purely diffusive case, $\bar{p}(x,t)$ satisfies the diffusion equation.

The stochastic models we are using on either side of the interface at $x = 0$ both provide an approximation to $\bar{p}(x,t)$ (as $h \to 0$ and $\Delta t \to 0$). We need to choose the

coupling parameters so that these approximations join together smoothly—that is, they both give the same value of $\bar{p}(0,t)$ and $\bar{p}_x(0,t)$, where the subscript indicates partial differentiation.

We label the compartment $[-kh, -kh+h]$ by k and denote the probability of finding a molecule in it by $p_k(t)h$ (so that $p_k(t)$ approximates the probability density function $\bar{p}(-kh+h/2, t)$ above). Since the inter-regime interface does not work in the same way as the interface between two neighbouring compartments, we generalize the transition rate from the compartments over the interface using the parameter Φ_1. As discussed in §2.1, this transition rate will be given as $\Phi_1 D/h^2$. If the molecule is transmitted, we have to decide where to place it: we suppose that it is placed at a random position in $x > 0$ with the probability distribution function $f(x)$ (so that it is placed in the interval $[x, x+dx]$ with probability $f(x)dx$).

We introduce parameters ψ_1 and ψ_2 to control the flux of molecules flowing from Ω_M to Ω_C as follows. Let us consider a system in which a molecule in Ω_M is absorbed from the interface (at $x = 0$) and placed in the corresponding compartment in Ω_C with a probability ψ_1 if, in a given time step, it generates a negative x coordinate (say $-x' < 0$) through the process of Brownian motion (using equation (1.2)). Such molecules are therefore reflected back into Ω_M with a probability $1 - \psi_1$ and, in such circumstances, placed at $x' > 0$. Furthermore, consider that a molecule starting at position $y' > 0$ is calculated to randomly appear at $x' > 0$ at the end of a given time step by equation (1.2). There is a probability that this molecule has, in this time step, crossed over the interface (at $x = 0$) and made its way back to $x' > 0$. This probability has been presented previously by Andrews & Bray [13] and is given by

$$P_m = \exp\left(-\frac{x'y'}{D\Delta t}\right). \tag{A 1}$$

We consider, for a full description of the interface as it is seen by molecules in Ω_M, that, along with the probability ψ_1 to absorb molecules at the interface from Ω_M, we also absorb molecules with a probability $\psi_2 P_m(x',y')$, where $\psi_2 \in [0,1]$ is another parameter of the method.

If we denote by $p(x,t)$ the probability density function of the discrete-time molecular-based algorithm, then these transmission/reflection rules are implemented in the following way:

$$p_1(t+\Delta t) = \left(1 - \frac{D\Delta t}{h^2}\right)p_1(t) + \frac{D\Delta t}{h^2}p_2(t)$$
$$- \Phi_1 \frac{D\Delta t}{h^2}p_1(t)$$
$$+ \int_0^\infty \int_0^\infty \frac{\psi_1 p(y,t)}{h\sqrt{4\pi D\Delta t}}\exp\left(\frac{-(x+y)^2}{4D\Delta t}\right)dxdy$$
$$+ \int_0^\infty \int_0^\infty \frac{\psi_2 P_m(x,y)p(y,t)}{h\sqrt{4\pi D\Delta t}}\exp\left(\frac{-(x-y)^2}{4D\Delta t}\right)dxdy$$
$$\tag{A2}$$

and

$$p(x,t+\Delta t) = \int_0^\infty \frac{p(y,t)}{\sqrt{4\pi D\Delta t}}\left[(1-\psi_1)\exp\left(\frac{-(x+y)^2}{4D\Delta t}\right)\right.$$
$$\left. + (1-\psi_2 P_m(x,y))\exp\left(\frac{-(x-y)^2}{4D\Delta t}\right)\right]dy$$
$$+ \frac{D\Delta t\Phi_1}{h}p_1(t)f(x). \tag{A 3}$$

The first and third terms of (A 2) represent the loss of molecules in a given time step from the interfacial compartment 1 into Ω_M and compartment 2. The second term in (A 2) represents the addition of molecules into the interfacial compartment 1 from compartment 2 by standard-compartment-based jumping. The fourth and fifth terms in (A 2) represent those molecules that are introduced into compartment 1 from Ω_M by the methods described by the probabilities ϕ_1 and ϕ_2, respectively. The integral in (A 3) represents the change in the probability density to find molecules in Ω_M owing to diffusion, including losses to compartment 1 by both of the methods described by the probabilities ϕ_1 (in term 1 of the integrand) and ϕ_2 (in term 2 of the integrand). The final term in (A 3) represents the addition of molecules from compartment 1 distributed into Ω_M according to the distribution $f(x)$. Denoting $\Phi_2 = \psi_1 + \psi_2$ and using (A 1), equations (A 2) and (A 3) can be rewritten as follows:

$$p_1(t+\Delta t) = \left(1 - \frac{D\Delta t}{h^2}\right)p_1(t) + \frac{D\Delta t}{h^2}p_2(t)$$
$$- \Phi_1 \frac{D\Delta t}{h^2}p_1(t)$$
$$+ \int_0^\infty \int_0^\infty \frac{\Phi_2 p(y,t)}{h\sqrt{4\pi D\Delta t}}\exp\left(\frac{-(x+y)^2}{4D\Delta t}\right)dxdy$$
$$\tag{A4}$$

and

$$p(x,t+\Delta t) = \int_0^\infty \frac{p(y,t)}{\sqrt{4\pi D\Delta t}}$$
$$\left[\exp\left(\frac{-(x-y)^2}{4D\Delta t}\right) + (1-\Phi_2)\exp\left(\frac{-(x+y)^2}{4D\Delta t}\right)\right]dy$$
$$+ \frac{D\Delta t\Phi_1}{h}p_1(t)f(x), \tag{A 5}$$

where $0 \leq \Phi_2 \leq 2$. Note that if $f(x)$ vanishes away from $x = 0$, then equation (A 5) reduces to the Fokker–Planck equation for finite-time-step Brownian motion and thus to the diffusion equation in the limit $\Delta t \to 0$. However, in the vicinity of $x = 0$, there is a boundary layer of width $O(\sqrt{\Delta t})$ [18]. We rescale (A 4) and (A 5) using the (dimensionless) boundary layer coordinate $\eta = x/\sqrt{D\Delta t}$. We also denote the probability density and placement function in this boundary layer region by $p_{inner}(\eta, t) = p(\sqrt{D\Delta t}\,\eta, t)$ and $f_{inner}(\eta) = \sqrt{D\Delta t}f(\sqrt{D\Delta t}\,\eta)$. Note the rescaling of f, which is necessary to satisfy the normalization

condition $\int_0^\infty f(x)\mathrm{d}x = 1$ because (as we will see) f vanishes outside the boundary layer. Thus, in the boundary layer scalings, (A 4) and (A 5) become

$$p_1(t+\Delta t) = \left(1 - \frac{(1+\Phi_1)D\Delta t}{h^2}\right)p_1(t) + \frac{D\Delta t}{h^2}p_2(t)$$
$$+ \frac{\Phi_2\sqrt{D\Delta t}}{h}\int_0^\infty\int_0^\infty p_{\mathrm{inner}}(\xi,t)K(\eta+\xi)\,\mathrm{d}\eta\,\mathrm{d}\xi$$
$$\text{(A 6)}$$

and

$$p_{\mathrm{inner}}(\eta, t+\Delta t) = \frac{\sqrt{D\Delta t}\Phi_1}{h}p_1(t)f_{\mathrm{inner}}(\eta)$$
$$+ \int_0^\infty p_{\mathrm{inner}}(\xi,t)(K(\eta-\xi) + (1-\Phi_2)K(\eta+\xi))\,\mathrm{d}\xi,$$
$$\text{(A 7)}$$

where $K(x) = (4\pi)^{-1/2}\exp(-x^2/4)$. Now in order for our two models to join smoothly, we require on the compartment-based side that

$$p_1(t) \sim \bar{p}\left(\frac{-h}{2}, t\right) = \bar{p}(0,t) - \frac{h}{2}\bar{p}_x(0,t) + \cdots$$

and

$$p_2(t) \sim \bar{p}\left(\frac{-3h}{2}, t\right) = \bar{p}(0,t) - \frac{3h}{2}\bar{p}_x(0,t) + \cdots,$$

while, for the molecular-based side, we want no rapid variation in the boundary layer, so that

$$p_{\mathrm{inner}}(\eta,t) \sim \bar{p}(0,t) + \sqrt{D\Delta t}(\eta+C)\bar{p}_x(0,t) + \cdots. \quad \text{(A 8)}$$

We have allowed here for a small shift C in where the molecular-based region 'sees' the interface; we will see that this extra degree of freedom is crucial. Equivalently we could have said that $p_k(t)$ approximates $\bar{p}(-kh + h/2 - C\sqrt{D\Delta t}, t)$ rather than $\bar{p}(-kh + h/2, t)$: C is really a small phase shift between the spatial coordinate in the two regions. Substituting these expansions into (A 6) and (A 7) and equating coefficients of h^0 and h^1 (with $h \sim \sqrt{\Delta t}$ as $h, \sqrt{\Delta t} \to 0$) gives

$$\Phi_1 = \frac{h\Phi_2}{\sqrt{D\Delta t}}\int_0^\infty\int_0^\infty K(\eta+\xi)\,\mathrm{d}\eta\,\mathrm{d}\xi = \frac{h\Phi_2}{\sqrt{D\Delta t\pi}}, \quad \text{(A 9)}$$

$$\Phi_1 = 2 - 2\Phi_2\int_0^\infty\int_0^\infty(\xi+C)K(\eta+\xi)\,\mathrm{d}\eta\,\mathrm{d}\xi$$
$$= 2 - \Phi_2 - \frac{2\Phi_2 C}{\sqrt{\pi}}, \quad \text{(A 10)}$$

$$1 = \int_0^\infty(K(\eta-\xi) + (1-\Phi_2)K(\eta+\xi))\,\mathrm{d}\xi$$
$$+ \frac{\sqrt{D\Delta t}\,\Phi_1}{h}f_{\mathrm{inner}}(\eta)$$
$$= 1 - \frac{\Phi_2}{2}\mathrm{erfc}\left(\frac{\eta}{2}\right) + \frac{\sqrt{D\Delta t}\Phi_1}{h}f_{\mathrm{inner}}(\eta), \quad \text{(A 11)}$$

and

$$\eta + C = \int_0^\infty(\eta+C)(K(\eta-\xi) + (1-\Phi_2)K(\eta+\xi))\,\mathrm{d}\xi$$
$$- \frac{\Phi_1}{2}f_{\mathrm{inner}}(\eta)$$
$$= \eta + C + (2-\Phi_2)\left(\frac{e^{-\eta^2/4}}{\sqrt{\pi}} - \frac{\eta}{2}\mathrm{erfc}\left(\frac{\eta}{2}\right)\right)$$
$$- \frac{C\Phi_2}{2}\mathrm{erfc}\left(\frac{\eta}{2}\right) - \frac{\Phi_1}{2}f_{\mathrm{inner}}(\eta). \quad \text{(A 12)}$$

From (A 9) we find

$$\frac{\Phi_1}{\Phi_2} = \frac{h}{\sqrt{\pi D\Delta t}}. \quad \text{(A 13)}$$

Then (A 11) gives

$$f_{\mathrm{inner}}(\eta) = \frac{\sqrt{\pi}}{2}\mathrm{erfc}\left(\frac{\eta}{2}\right), \quad \text{(A 14)}$$

corresponding to the unscaled

$$f(x) = \sqrt{\frac{\pi}{4D\Delta t}}\,\mathrm{erfc}\left(\frac{x}{\sqrt{4D\Delta t}}\right), \quad \text{(A 15)}$$

which is denoted as equation (2.2) in the paper. The normalization condition on f is automatically satisfied.

Substituting (A 14) and (A 10) into (A 12) gives

$$0 = (2-\Phi_2)\left(\frac{e^{-\eta^2/4}}{\sqrt{\pi}} - \frac{\eta}{2}\mathrm{erfc}\left(\frac{\eta}{2}\right) - \frac{\sqrt{\pi}}{4}\mathrm{erfc}\left(\frac{\eta}{2}\right)\right),$$

from which we find

$$\Phi_2 = 2. \quad \text{(A 16)}$$

Because $\Phi_2 = \psi_1 + \psi_2$, where ψ_1 and ψ_2 are probabilities, the only option is that both ψ_1 and ψ_2 are equal to 1. This justifies the use of equation (2.3) in the TRM, because equation (2.3) is the probability given by (A 1). Substituting (A 16) in (A 9), we derive the formula for Φ_1, which is presented as equation (2.1) in the paper. Finally, substituting this value into (A 10) gives

$$C = -\frac{h}{2\sqrt{D\Delta t}}. \quad \text{(A 17)}$$

One interpretation of this value of C is that we should think of $p_k(t)$ as approximating $\bar{p}(-kh + h, t)$, so that $p_1(t)$ approximates $\bar{p}(0, t)$ and not $\bar{p}(-h/2, t)$.

REFERENCES

1 Erdmann, T., Howard, M. & ten Wolde, P. R. 2009 The role of spatial averaging in the precision of gene expression patterns. *Phys. Rev. Lett.* **103**, 258101. (doi:10.1103/PhysRevLett.103.258101)

2 Takahashi, K., Tănase-Nicola, S. & ten Wolde, P. R. 2010 Spatio-temporal correlations can drastically change the response of a MAPK pathway. *Proc. Natl Acad. Sci. USA* **107**, 19 820–19 825. (doi:10.1073/pnas.0906885107)

3 Lipkow, K., Andrews, S. S. & Bray, D. 2005 Simulated diffusion of phosphorylated CHeY through the cytoplasm of *Escherichia coli. J. Bacteriol.* **187**, 45–53. (doi:10.1128/JB.187.1.45-53.2005)

4 Fange, D. & Elf, J. 2006 Noise-induced Min phenotypes in *E. coli*. *PLoS Comput. Biol.* **2**, 637–648. (doi:10.1371/journal.pcbi.0020080)

5 Tomita, M. 2001 Whole-cell simulation: a grand challenge of the 21st century. *Trends Biotechnol.* **19**, 205–210. (doi:10.1016/S0167-7799(01)01636-5)

6 Murray, J. D. 2003 *Mathematical biology II: spatial models and biomedical applications*, pp. 403–420. Berlin, Germany: Springer.

7 Erban, R. & Chapman, J. 2009 Stochastic modelling of reaction–diffusion processes: algorithms for bimolecular reactions. *Phys. Biol.* **6**, 046001. (doi:10.1088/1478-3975/6/4/046001)

8 Fange, D., Berg, O. G., Sjöberg, P. & Elf, J. 2010 Stochastic reaction–diffusion kinetics in the microscopic limit. *Proc. Natl Acad. Sci. USA* **107**, 19 820–19 825.(doi:10.1073/pnas.1006565107)

9 Hattne, J., Fange, D. & Elf, J. 2005 Stochastic reaction–diffusion simulation with MesoRD. *Bioinformatics* **21**, 2923–2924. (doi:10.1093/bioinformatics/bti431)

10 Ander, M. 2004 SmartCell, a framework to simulate cellular processes that combines stochastic approximation with diffusion and localisation: analysis of simple networks. *Syst. Biol.* **1**, 129–138. (doi:10.1049/sb:20045017)

11 Isaacson, S. A. 2009 The reaction–diffusion master equation as an asymptotic approximation of diffusion to a small target. *SIAM J. Appl. Math.* **70**, 77–110. (doi:10.1137/070705039)

12 Isaacson, S. A. & Isaacson, D. 2009 Reaction–diffusion master equation, diffusion-limited reactions, and singular potentials. *Phys. Rev. E* **80**, 066106. (doi:10.1103/PhysRevE.80.066106)

13 Andrews, S. S. & Bray, D. 2004 Stochastic simulation of chemical reactions with spatial resolution and single molecular detail. *Phys. Biol.* **1**, 137–151. (doi:10.1088/1478-3967/1/3/001)

14 Andrews, S. S., Addy, N. J., Brent, R. & Arkin, A. P. 2010 Detailed simulations of cell biology with Smoldyn 2.1. *PLoS Comput. Biol.* **6**, e1000705. (doi:10.1371/journal.pcbi.1000705)

15 Stiles, J. R. & Bartol, T. M. 2001 Monte Carlo methods for simulating realistic synaptic microphysiology using MCell. In *Computational neuroscience: realistic modeling for experimentalists* (ed. E. De Schutter), pp. 87–127. Boca Raton, FL: CRC Press.

16 Kerr, R. A., Bartol, T. M., Kaminsky, B., Dittrich, M., Chang, J.-C. J., Baden, S. B., Sejnowski, T. J. & Stiles, J. R. 2008 Fast Monte Carlo simulation methods for biological reaction–diffusion systems in solution and on surfaces. *SIAM J. Sci. Comput.* **30**, 3126–3126. (doi:10.1137/070692017)

17 van Zon, J. S. & ten Wolde, P. R. 2005 Simulating biochemical networks at the particle level and in time and space: Green's function reaction dynamics. *Phys. Rev. Lett.* **94**, 128103. (doi:10.1103/PhysRevLett.94.128103)

18 Erban, R. & Chapman, J. 2007 Reactive boundary conditions for stochastic simulations of reaction–diffusion processes. *Phys. Biol.* **4**, 16–28. (doi:10.1088/1478-3975/4/1/003)

19 Erban, R., Chapman, J. & Maini, P. 2007 A practical guide to stochastic simulations of reaction–diffusion processes. (http://arxiv.org/abs/0704.1908)

20 Tomita, M. *et al.* 1999 E-Cell software environment for whole-cell simulation. *Bioinformatics* **15**, 72–84. (doi:10.1093/bioinformatics/15.1.72)

21 Gillespie, D. 1977 Exact stochastic simulation of coupled chemical reactions. *J. Phys. Chem.* **81**, 2340–2361. (doi:10.1021/j100540a008)

22 Gibson, M. & Bruck, J. 2000 Efficient exact stochastic simulation of chemical systems with many species and channels. *J. Phys. Chem. A* **104**, 1876–1889. (doi:10.1021/jp993732q)

23 Lipkova, J., Zygalakis, K. C., Chapman, S. J. & Erban, R. 2011 Analysis of Brownian dynamics simulations of reversible biomolecular reactions. *SIAM J. Appl. Math.* **71**, 714–730. (doi:10.1137/100794213)

24 Andrews, S. S. 2009 Accurate particle-based simulation of adsorption, desorption and partial transmission. *Phys. Biol.* **6**, 046015. (doi:10.1088/1478-3975/6/4/046015)

25 Crank, J. 1975 *The mathematics of diffusion*. Oxford, UK: Oxford University Press.

26 Tostevin, F., ten Wolde, P. R. & Howard, M. 2007 Fundamental limits of position determination by concentration gradients. *PLoS Comput. Biol.* **3**, 0763–0771.

27 Bergmann, S. *et al.* 2007 Pre-steady-state decoding of the bicoid morphogen gradient. *PLoS Comput. Biol.* **5**, 0232–0242.

28 Engblom, S., Ferm, L., Hellander, A. & Lötstedt, P. 2009 Simulation of stochastic reaction-diffusion processes on unstructured meshes. *SIAM J. Sci. Comput.* **31**, 1774–1797. (doi:10.1137/080721388)

29 Isaacson, S. A. & Peskin, C. S. 2007 Incorporating diffusion in complex geometries into stochastic chemical kinetics simulations. *SIAM J. Sci. Comput.* **28**, 47–74. (doi:10.1137/040605060)